# AN IMAGE ANALYSIS STUDY ON VARISTOR CERAMIC MICROSTRUCTURES CORRELATED TO THEIR ELECTROTHERMAL PERFORMANCES[1]

*José Geraldo de Melo Furtado* [2]
*Rodrigo Dias* [3]
*Maria Cecília de Souza Nóbrega* [4]
*Eduardo Torres Serra* [5]

**Abstract**

Varistors are very complex polycrystalline ceramic systems containing several dopants and their electrical properties are directly dependent on the chemical composition and on microstructural characteristics, such as grain size, porosity, twins and phase distribution. The aim of this work is to evaluate, using image analysis tools, the relations between microstructural characteristics and electrothermal performance of varistor ceramics. Varistor ceramics were electrical and microstructurally analyzed. The microstructural characterization was made by optical microscopy, scanning electron microscopy, and energy dispersive X-ray spectroscopy. Microstructural and morphological parameters were obtained by means image analysis techniques based on combinations of classical and appropriate filters. Segmentation and binarization methods were used to differentiate grain and grain boundaries properties, as well phase structures. In this study, image processing and measurements have been developed in order to extract the relevant microstructural parameters on the varistor ceramics. It was developed an appropriate filtering and segmentation method for analysis of varistor ceramics to obtain grain and grain boundaries structural and morphological informations. The obtained results show that conventional metal oxide-based varistor ceramics exhibit considerable heterogeneity and different types of grain boundary conditions, resulting in lower energy absorption capability and worst electrothermal behavior than rare-earth adding zinc oxide-based varistors.

**Key words:** Varistor ceramics; Image analysis; Microstructural characterization.

**UM ESTUDO DE ANÁLISE DE IMAGENS SOBRE MICROESTRUTURAS DE CERÂMICAS VARISTORAS CORRELACIONADAS AO SEU DESEMPENHO ELETROTÉRMICO**

**Resumo**

Varistores são complexos sistemas cerâmicos policristalinos contendo diversos dopantes e suas propriedades elétricas são diretamente dependentes da composição química e das características microestruturais, tais como tamanho de grão, porosidade, maclas e distribuição de fases. O objetivo deste trabalho é avaliar, usando métodos de análise de imagens, as relações entre características microestruturais e o desempenho eletrotérmico das cerâmicas varistoras caracterizadas microestrutural e eletricamente. A caracterização microestrutural foi feita por microscopia eletrônica de varredura e de transmissão e espectroscopia de raios-X por dispersão de energia. Parâmetros microestruturais e morfológicos foram obtidos por técnicas de análises de imagens baseadas em filtros apropriados. Métodos de segmentação e binarização foram usados para diferenciar propriedades dos grãos e dos contornos de grão, bem como a presença de fases secundárias, proporcionando a obtenção de informações estruturais e morfológicas. Os resultados obtidos mostram que as cerâmicas varistoras convencionais exibem considerável heterogeneidade e diferentes tipos de condições nos contornos de grão, resultando em menor capacidade de absorção de energia e pior comportamento eletrotérmico do que as cerâmicas varistoras à base de óxido de zinco dopadas com terras-raras.

**Palavras-chave**: Cerâmicas varistoras; Análise de imagens; Microestrutura.

[1] *Technical contribution to 63rd ABM Annual Congress, July, 28th to August 1st, 2008, Curitiba – PR – Brazil.*

[2] *D.Sc., Researcher, Special Technologies Department (DTE), Electric Power Research Center, CEPEL, P.O.Box 68007, 21940-970, Rio de Janeiro, Brazil. e-mail: furtado@cepel.br*

[3] *Laboratory Technician, DTE, Electric Power Research Center, CEPEL, Rio de Janeiro, Brazil.*

[4] *D.Sc., Professor, Department of Metallurgical and Materials Engineering, Federal University of Rio de Janeiro, P.O.Box 68505, 21945-970, Rio de Janeiro, Brazil.*

[5] *D.Sc., Research Consultant, R&D Directorate, Electric Power Research Center, CEPEL, Rio de Janeiro, Brazil*

## 1 INTRODUCTION

Zinc oxide (ZnO) varistors (*vari*able resi*stors*) are polycrystalline ceramic devices exhibiting highly nonlinear (non-ohmic) electrical behavior and greater energy absorption capabilities.[1,2] The industrial fabrication of ZnO varistors is done by mixing semiconducting ZnO powder with other ceramic powders such as Bi, Co, Mn, and Pr oxides, and subjecting the powder mixture to conventional ceramic pressing and generally liquid-phase sintering techniques.[3] The sintering results in a polycrystalline ceramic with a singular grain boundary property which produces the nonlinear current-voltage (I-V) characteristics of the device (2). Microstructurally, the ZnO varistors are comprised of semiconducting n-type ZnO grains, surrounded by very thin ($1\text{-}10^{-3}$ $\mu$m) insulating intergranular layers.[1] Several conduction mechanisms for the varistor have been proposed based on this ceramic microstructure,[1,2,4] which has led to varistor behavior being widely interpreted as resulting from the series-parallel network formed by ZnO-ZnO homojunctions and ZnO grains-intergranular-phase junctions.[2,5] Capacitance measurements as a function of voltage have supported the model of Schottky barriers at grain boundaries.[6] Electrically, the varistors show highly nonlinear I-V characteristics similar to the back-to-back Zener diode, but with much higher voltage, current, and energy handling capabilities.[1] As a result, they are widely used employed in transient voltage surge protection applications, such as surge absorbers in electronic circuits and core elements of surge arresters in electric power systems,[3] and to do so repeatedly without being destroyed.[2,3]

The electrical characteristics of a varistor are altered after some time under electrical bias. This behavior is known as degradation phenomena and manifests itself mainly by alterations of the electric varistor curve.[3] As a result, the varistors have a tendency of increasing in leakage current, in the permanent polarization regime, with increasing time and temperature. Thus, the load life of ZnO varistors is restricted by the electrothermal runaway because of the increase of the leakage current under electric load. In conditions of surge incidence, when the device needs to absorb large energy, this behavior tends to become uncontrolled. Therefore, the reduction of the leakage current and the increases of energy absorption capability are important problems of the varistor technology[2] and can be reached by the adequate control of the microstructural parameters, such as grain boundary chemical composition, grain size distribution, densification level, and phase structure.[5]

ZnO-based varistor ceramics are divided generally into two categories, called $Bi_2O_3$-based and $Pr_6O_{11}$-based varistors, in terms of varistor-forming oxides inducing the nonlinear properties of varistors.[3] Most of the commercial ZnO varistors are $Bi_2O_3$-based varistors, which have been mainly studied in various aspects since ZnO varistors were discovered by Matsuoka, Masuyama e Ida.[7] However, $Bi_2O_3$-based ZnO varistors are not suitable to be used in multilayer chip varistors manufacture, due to $Bi_2O_3$ having a high volatility and reactivity.[8] Furthermore, in general, $Bi_2O_3$-based ZnO varistors possess four phases, namely ZnO grains, Bi-rich intergranular layers, an additional insulating spinel phase, which does not play any role in electrical conduction, and pyrochlore phase. On the other hand, in $Pr_6O_{11}$-based ZnO varistors only two phases are present in a sintered body, namely, ZnO grains and the intergranular phase composed mainly of praseodymium oxide.[2,8] The absence of a spinel phase increases the active grain boundary through which the electrical current flows. Therefore, the effective cross-section area of the element is increased.[8] Earlier studies about $Pr_6O_{11}$-based varistors have been limited to the ternary system

$ZnO$-$Pr_6O_{11}$-$CoO$ and dissimilarities between $Bi_2O_3$-based and $Pr_6O_{11}$-based ZnO varistors.[8-11] Recently, many works have been made in order to study the influence of other rare-earth oxides (such as $Y_2O_3$, $Nd_2O_3$, $Er_2O_3$, and $Dy_2O_3$) on the microstructural and electrical properties of the ternary system $ZnO$-$Pr_6O_{11}$-$CoO$.[12,13] The varistors produced have exhibited a relatively good electrical performance.

Earlier studies in ZnO varistors have shown that the narrow regions, where the sintered grains have grown together, control the resistance of the entire sample (2, 4). In those regions, the surface/volume ratio is sufficiently high for the acceptor concentration (which occurs because of adsorbed oxygen) to exceed the donor concentration inside the ZnO grains.[2] More recent works have shown that Schottky barriers result from interface states because of the chemisorbed oxygen ion at the ZnO-ceramic grain boundaries.[14,15] Although the microstructure of ZnO-based varistors exhibit considerable variation from one manufacturer to another, they all exhibit the characteristics of a typical ceramic prepared by liquid-phase sintering, consisting mainly of large ZnO grains with a varistor former-rich second phase at the nodal points (triple junctions) and/or intergranular layer (IGL) regions. In the present work an evaluation of the microstructural characteristics by image analysis of the ZnO-based varistor ceramics, whose chemical compositions are shown in Table 1, was made and applied to the understanding of the varistor performance.

**Table 1** - Chemical composition of the varistor ceramic investigated systems.

| Designation | Chemical composition (mol%) |
|---|---|
| ZB | $96.5{\cdot}ZnO\text{-}0.5{\cdot}Bi_2O_3\text{-}1.0{\cdot}Sb_2O_3\text{-}1.0{\cdot}CoO\text{-}0.5{\cdot}MnO\text{-}0.5{\cdot}Cr_2O_3$ |
| ZP | $98.5{\cdot}ZnO\text{-}1.0{\cdot}CoO\text{-}0.5{\cdot}Pr_6O_{11}$ |
| ZPC | $97.59{\cdot}ZnO\text{-}1.00{\cdot}Pr_6O_{11}\text{-}1.00{\cdot}Co_3O_4\text{-}0.20{\cdot}B_2O_3\text{-}0.20{\cdot}CaO\text{-}0.01{\cdot}Al_2O_3$ |
| ZPNC | $97.3{\cdot}ZnO\text{-}0.5{\cdot}Pr_6O_{11}\text{-}1.0{\cdot}Co_3O_4\text{-}1.0{\cdot}Nd_2O_3\text{-}0.2{\cdot}Cr_2O_3$ |

## 2 EXPERIMENTAL

Appropriate weights of analytical reagent grade powders were used to prepare the ZnO based ceramics. The sample compositions are shown in Table I above. The powders with adequate compositions were ball milled with zirconia balls in isopropyl alcohol media inside of a zirconia jar for 24 h. The resultant mixture was dried at 110°C for 12 h and calcined in air at 750°C for 2 h. The calcined mixture was granulated in a 200 mesh sieve and pressed into discs of 12.4 mm in diameter and 2.1 mm in thickness at a pressure of 80 MPa. The discs were sintered at 1.200°C–1350°C in air atmosphere for 1 h. The heating and cooling rates were 5°C/min. The average size of the final samples was 10.2 mm in diameter and 1.1 mm in thickness. The sintered bodies were sanded and polished, silver paste was coated on both faces of the samples and the silver electrode was formed by heating at 600°C for 10 min. The area of the electrodes was approximately 0.212 $cm^2$. The electrothermal behavior is associated to energy absorption capability (EAC) which were inferred from the dielectric characterization of the varistor ceramic blocks compared to a thermal model considered[16] using a curve tracer source-measurement unit (Tektronix 577). For these measurements, in all the results that follow the EAC average values were obtained from four samples of each system under study.

The sample microstructures were examined by scanning electron microscopy (SEM, ZEISS DSM 960) applied on the polished and 6M-NaOH aqueous solution-etched (5 min) surface of samples, as well as on the fractured surface of the samples, and by transmission electron microscopy (TEM, JEOL 2000 FX). The grain sizes were determined by linear semi-automatic intercept method.[17,18] The compositional analysis of the selected areas was determined by an attached X-ray energy dispersive spectroscopy (EDS, Oxford ISIS) system. The crystalline phases were identified by powder X-ray diffraction (XRD, Diano XRD-8545, $\lambda$CuK$\alpha$ radiation). The density of the varistor ceramics was measured by the Archimedes method and by image analysis techniques.[18] The procedures for Image analysis were implemented in Image-Pro Plus 6.0 (Media Cybernetics, 2006) software. The evolution of the resistive component of the leakage current ($I_{LR}$) with respect to time (at constant temperature of 100°C) was estimated from the equation:

$$\Delta I_{LR} = I_{LR}(t) - I_{LR}(0) = K_R t^n \qquad (A)$$

where $\Delta I_{LR}$ is the time-dependent increase in $I_{LR}$, $K_R$ is an effective rate constant, $I_{LR}(0)$ is $I_{LR}$ at time zero, and n a time exponent that gives a measure of the degree of stability of the device (for the most commercial varistors n is equal to 0.5).

## 3 RESULTS AND DISCUSSION

Figure 1 shows typical microstructural features of ZnO-based varistor ceramics, which, ideally, consists mainly of n-type semiconductor grains and grain boundaries (ZnO homojunctions, cf. Figure 1(b)). However, real microstructures produced by liquid phase sintering processes, as presented in Figure 1(a), results in the formation of intergranular layers and secondary precipitate phases depending of the chemical composition. The IGLs, ideally, must be thin and ceramic microstructure must be full-densified (low porosity) for minimize the leakage current.[2,3] In fact, the ideal grain boundary junctions, as shown in Figures 1(a), 1(c), 2(b) and 2(c), behave like "micro-varistors", therefore already presents a varistor behavior. Figure 2(a) shows the formation of very dimensional heterogeneous IGLs and, in general, ZnO varistor microstructures also have great presence of twins (Figure 1(a)).

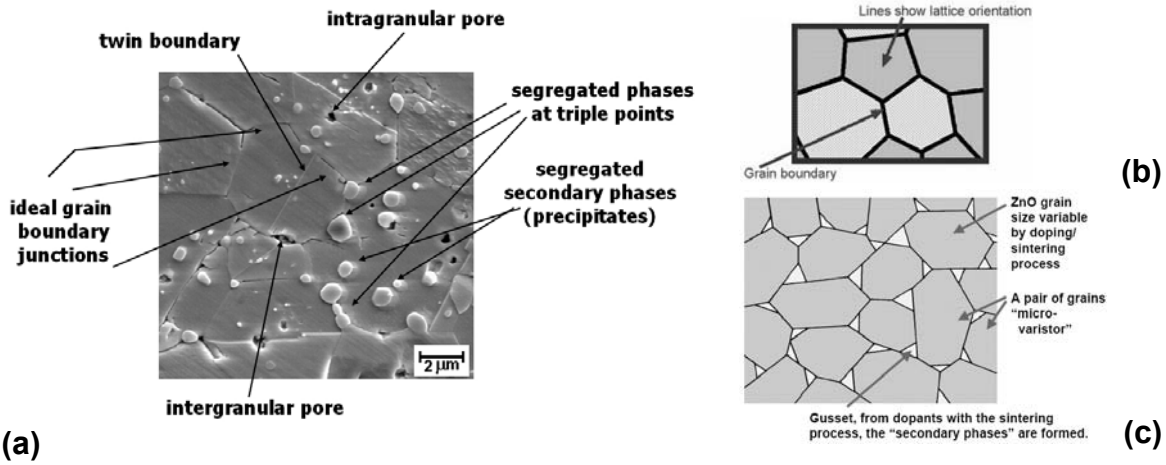


**Figure 1.** (a) Typical microstructural characteristics of a ZnO-based varistor ceramic; (b) scheme showing lattice orientation and grain boundaries in ZnO ceramics; (c) simplified scheme of the microstructure of a ZnO-based varistor ceramic.

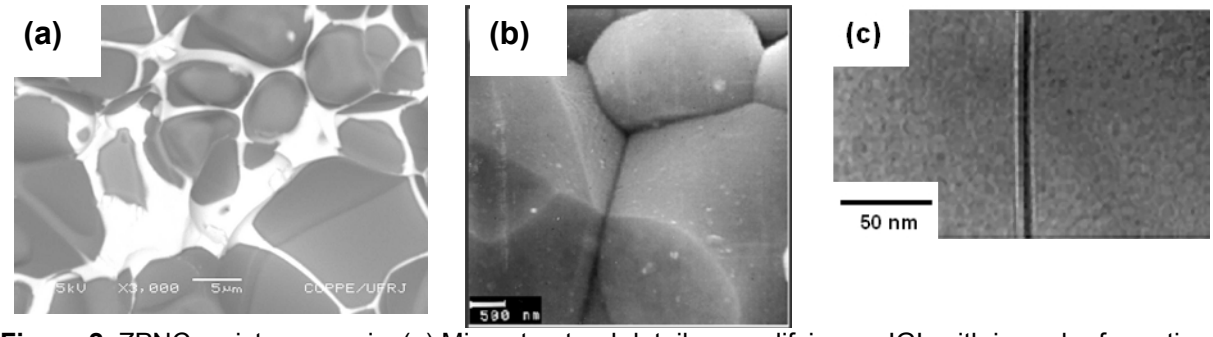


**Figure 2.** ZPNC varistor ceramic: (a) Microstructural detail exemplifying an IGL with irregular formation (cluster); (b) SEM micrograph of magnified detail of the microstructure showing that ZnO grains are in direct contact with each other; (c) TEM micrographs emphasizing the grain boundary region (with IGL).

Figure 3 shows comparatively examples of microstructure of the ZB and ZPC ceramics. ZPC presents more densified aspect, as well greater physical-chemical homogeneity than ZB. Additionally, Figure 4 shows the XRD patterns of sintered ZB (evidencing its multiphase structure, including spinel and $\gamma$-$Bi_2O_3$ phases) and ZP (presents only ZnO and Pr-rich phases) varistor ceramic systems.

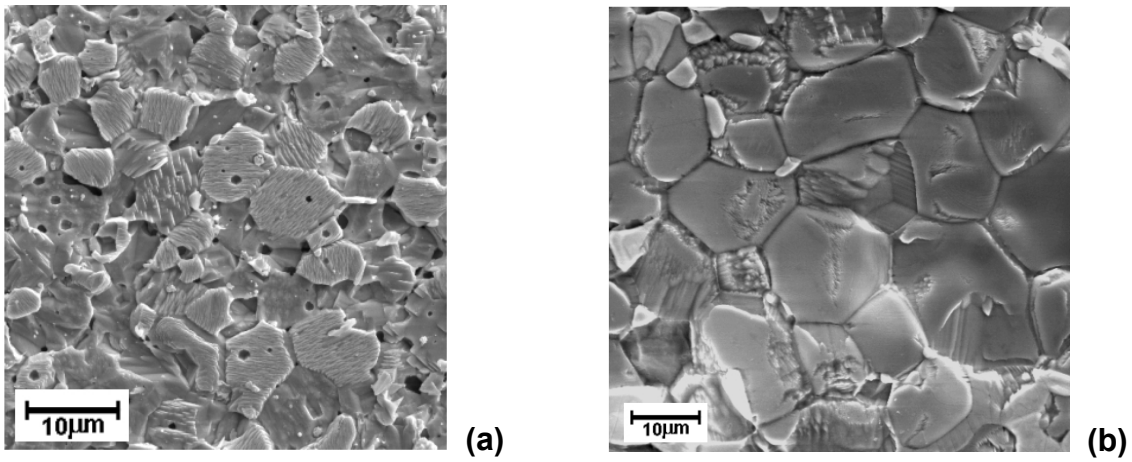


**Figure 3.** Examples of ZnO-based varistor ceramic microstructures: (a) Conventional ($Bi_2O_3$-based) - ZB; (b) Earth-rare monodoped ($Pr_6O_{11}$-based) - ZPC.

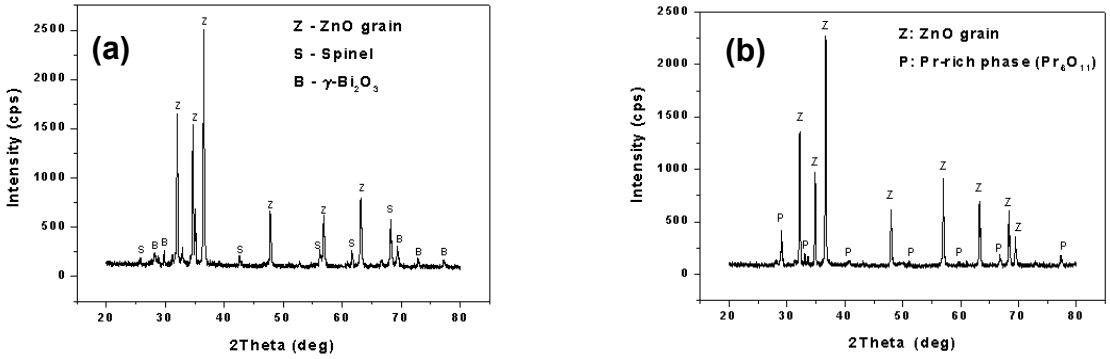


**Figure 4.** X-ray diffraction (XRD) patterns of (a) ZB sintered at 1.200°C, and (b) ZP sintered at 1.300°C varistor ceramic systems.

Figures 5 and 6 show the results of a SEM-EDS analysis (point, line and mapping) of a ZP ceramic evidencing the selective dopant distribution. In fact, the Pr distribution is essentially complementary to that of the Zn, since Pr not forms solid solution with the ZnO according to its larger ionic radius, being an IGL former.[8]

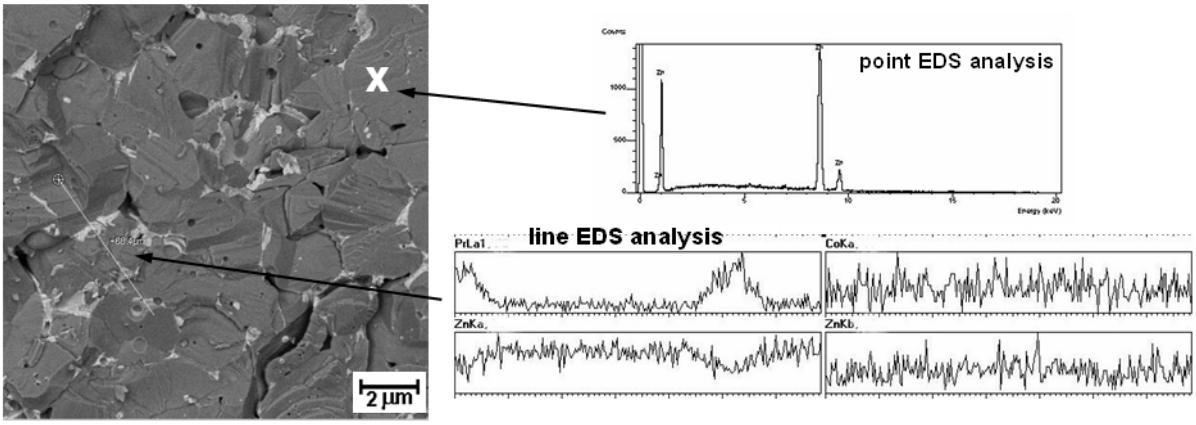


**Figure 5.** SEM-EDS analysis of a ZnO-based varistor ceramic (ZP) showing a point EDS spectrum characteristic of the ZnO grain core (bulk phase) and a line EDS analysis evidencing the complementary distribution of the Pr dopant.

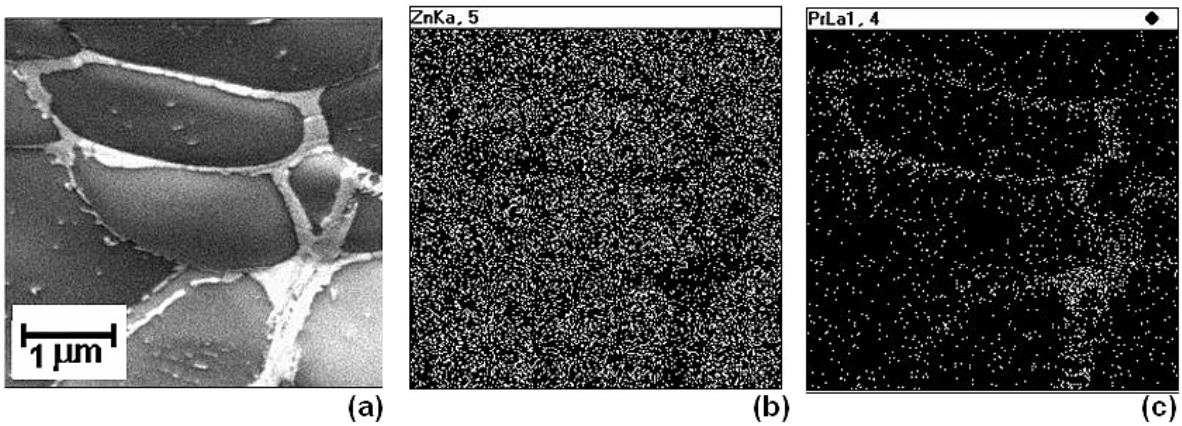


**Figure 6.** SEM-EDS mapping of the ZP varistor ceramic showing the complementary and specific distribution of the Pr dopant which results in the IGL formation.

Additionally, the Figure 7(a) shows a SEM photomicrograph of the polished and chemical etched surface (leached) of the ZPNC ceramic sintered at 1.300°C and Figure 7(b) shows in detail the X-Z-marked region. The X, Y and Z marks (Figure 7) indicate the specific regions to qualitative EDS analyses (Figure 8), denoting, respectively, a ZnO grain, a very thin IGL (grain boundaries region) and an IGL region, whose EDS patterns are shown, respectively, in the Figures 8(a), 8(b) and 8(c). In Figure 8(c) can be seen that, in fact, the IGL region contains a high concentrations of rare-earth elements (Pr and Nd) and smaller amounts of Cr and Co. However, as can be seen in the Figures 2(a) and 7, the intergranular layer distribution is heterogeneous, because regions exist that ZnO grains are in direct contact with each other (cf. Figure 2(b)). The heterogeneous distribution of the Pr-Nd-rich intergranular material observed, mainly in Figure 7, suggests that processing conditions are not optimized yet, and the ZnO grains were not suffered an uniform wetting by liquid phase-varistor former rare-earth mixture, although the resultant varistor ceramic samples have presented excellent electrothermal performance (cf. Figure 10). In fact, the uniform distribution of grain boundary materials (varistor formers and dopants) can be expected to improve significantly the performance of ceramics which are liquid-phase sintered and this is believed to result in the proper conditioning required to form the electrically active junctions in the large majority of the grain boundary regions such as shown the enlarged SEM micrograph of the triple

point of the ZPNC sample (Figure 2(b)).[2,8] Thus, from these observations, it is reasonable that the varistor electrical behavior of ZPNC ceramics can be considerably improved by means of the increase of its microstructural homogeneity.

Figure 9 shows SEM photomicrographs and respective image processed results showing microstructural specific features of some studied varistor ceramics, exemplifying image analysis procedures, through of the use of filtering and segmentation methods, which were used to extract the relevant microstructural parameters (mainly grain size and densification level) on the varistor ceramic photomicrographs, and allowed to relate these microstructural characteristics with the electrothermal performance (in terms of EAC) of the devices as shown in the graphs presented in the Figure 10.

On the EAC it is verified by analysis of the Figures 10(a) and 10(b) that for all the systems studied the EAC increases with the increase of the densification degree and of the average grain size characteristic of the varistor microstructure. However, for all studied formulations the increase of the EAC to average grain size greater than 8.5 μm is significantly reduced (Figure 10(b)). This fact usually is not a problem, because varistors presenting average grain size above this value do not usually requested by high values of energy. Meanwhile, mainly for high voltage applications, when is necessary high breakdown electric field, which depends on a microstructure characterized by reduced average grain size, this can be a challenge, so there is perspectives to compositional optimization of high voltage varistors. In fact, as shown in the graphs of Figure 10, the EAC depends not only on geometric and dimensional factors, but also on chemical composition (ceramic formulation), since the chemical composition influences the grain growth and densification kinetics. Moreover, depending on the chemical composition and on thermal treatments used different phase structures can be generated, as seen by comparing the ZB and rare-earth-based formulations (ZP, ZPC and ZPNC), since the ZB presents a multiphase structure and the others show more simple structure consisting essentially of two phases: ZnO grains (doped with Co) and rare-earth elements (Pr and Nd)-rich phase (doped with Cr and Co) segregated at grain boundaries.[8,19]

Corroborating the results of the EAC analysis, the Figure 11 shows the $\Delta I_{LR}$ time-dependent evolution curves and $K_R$ ($I_{LR}$ increment rate) obtained values for each system studied. This results indicates that the studied varistors are in the following descending order of stability: ZPNC, ZPC, ZP and ZB (in respect to leakage current increasing), which is the same descending order for the EAC (Figure 10), since the ZPNC system presented the slowest $I_{LR}$ growth (smaller $K_R$ values), since as much as bigger $K_R$ value, then greater will be the trend to electrothermal degradation of the device, inasmuch as the $\Delta I_{LR}$ will grow more quickly. In fact, the $K_R$ value to ZB is about 30% greater than the value to the ZPNC system.

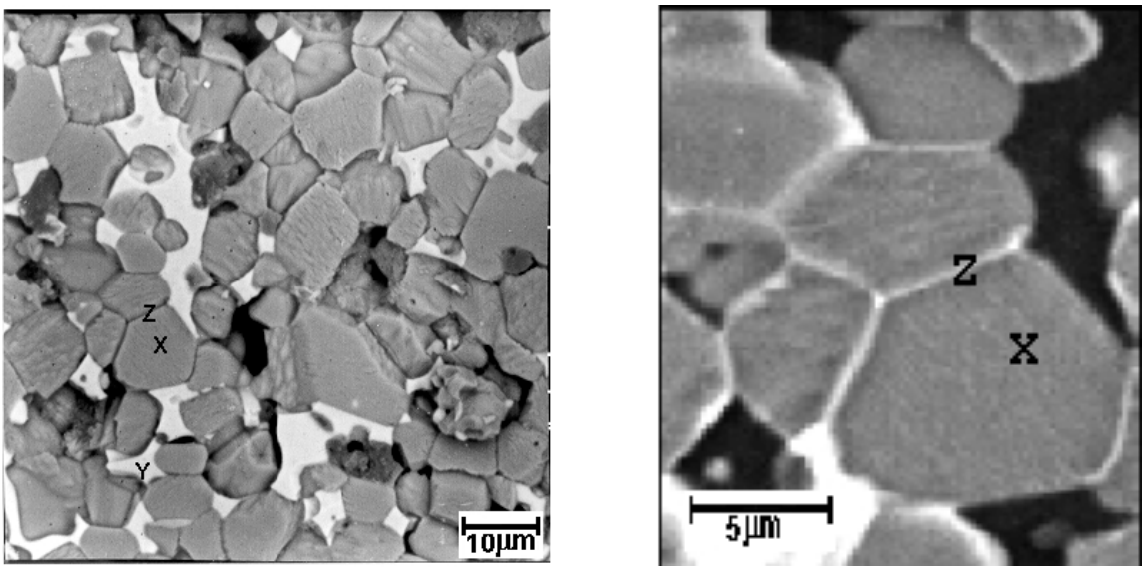


(a) (b)

**Figure 7.** (a) SEM micrograph of the polished and etched surface of the ZPNC ceramic sintered at 1300$^0$C; (b) X-Z-marked region in detail.

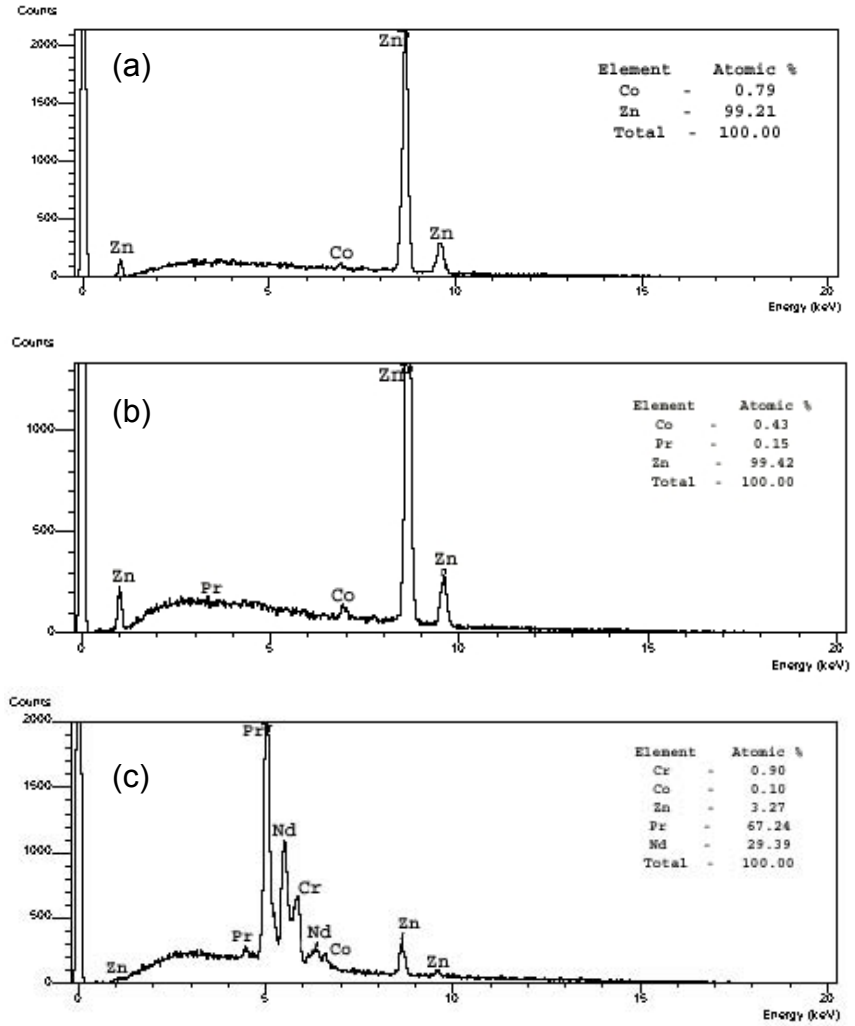


**Figure 8.** EDS analysis of ZPNC varistor ceramic: (a) ZnO grain (X-marked, Figure 6(a)), (b) Grain Boundary region (Z-marked, Figure 6(a)) and (c) IGL region (Y-marked, Figure 6(a)).

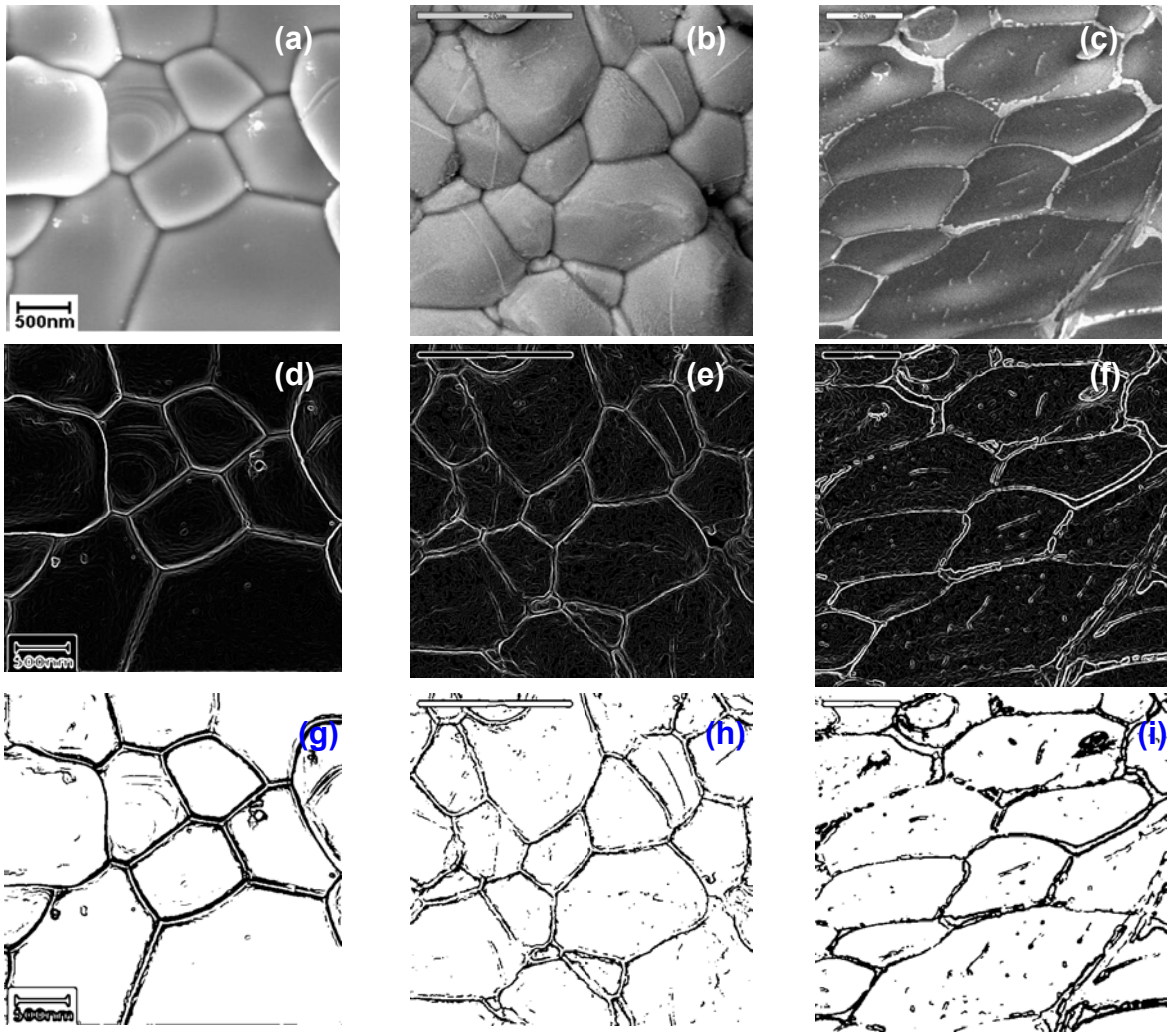


**Figure 9.** SEM photomicrographs of the full-densified microstructures and respective image processed results of some studied varistor ceramics: (a) ZPNC; (b) ZPC; (c) ZP; (d), (e) e (f) enhanced median filter and Sobel edge detection; (g), (h), (i) after segmentation process.

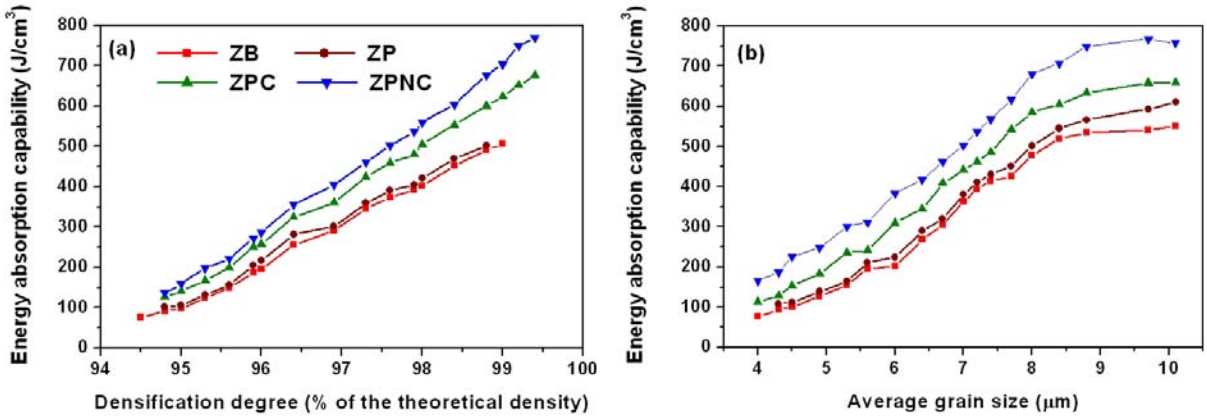


**Figure 10.** Electrothermal varistor performance related with its microstructural characteristics - energy absorption capability related to: (a) densification degree of the varistor block; (b) average grain size of the varistor microstructure.

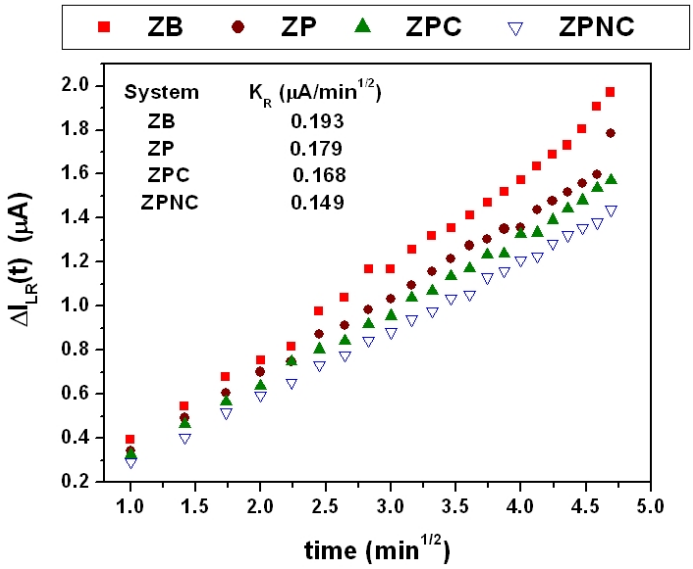


**Figure 11.** Electrothermal varistor performance: leakage current increment with respect to time (at constant temperature of 100°C), for the varistor ceramic systems studied.

## 4 CONCLUSIONS

It was verified that the zinc oxide-based varistor ceramics doped with rare-earth oxides showed greater energy absorption capability and lower leakage current than the conventional varistors, particularly in densification usual levels the ZPNC (97.3·ZnO-0.5·$Pr_6O_{11}$-1.0·$Co_3O_4$-1.0·$Nd_2O_3$-0.2·$Cr_2O_3$, mol%) ceramics exhibited the highest energy absorption capability. Additionaly, it was verified that the energy absorption capability depends on chemical composition, which influences the phase structure, although the main dependencies are in relation to densification degree and average grain size.

## REFERENCES


1 GUPTA, T. K. Application of zinc oxide varistors. **J. Am. Ceram. Soc.**, v.73, n.7, p. 1817-1840, 1990.

2 CLARKE, D. R. Varistor ceramics. **J. Am. Ceram. Soc.**, v.82, n.3, p. 485-502, 1999.

3 LAGRANGE, A. Present and Future of Zinc Oxide Varistors. In: **Electronic Ceramics**, edited by STEELE, B. C. H., Elsevier Applied Science, London, UK, p. 1-27, 1991.

4 MANTAS, P.Q., Baptista, J. L. The barrier height formation in ZnO varistors. **J. Europ. Ceram. Soc.**, v.15, p. 605-615, 1995.

5 LEVINSON, L. M., PHILIPP, H. R. The physics of metal oxide varistors. **J. Appl. Phys.**, v.46, n.3, p. 1332-1341, 1975.

6 EDA, K. Zinc oxide varistors. **IEEE Electrical Insulation Magazine**, v.5, n.6, p. 28-41, 1989.

7 MATSUOKA, M., MASUYAMA, T., IDA, Y. Nonohmic properties of zinc oxide ceramics. **Supp. J. Jpn. Soc. Appl. Phys.**, v.39, p. 94-101, 1970.

8 MUKAE, K. Zinc oxide varistors with praseodymium oxide. **Am. Ceram. Soc. Bull.**, v.66, n.9, p. 1329-1331, 1987.

9 NAHM, C-W. The electrical properties and d.c. degradation characteristics of $Dy_2O_3$ doped $Pr_6O_{11}$-based ZnO varistors. **J. Europ.Ceram. Soc.**, v.21, p. 545-553, 2001.
10 CHUN, S-Y., WAKIYA, N., FUNAKUBO, H., SHINOZAKI, K., MIZUTANI, N. Phase diagram and microstructure in the ZnO-$Pr_2O_3$ system. **J. Am. Ceram. Soc.**, v.80, n.4, p. 995-998, 1997.
11 MUKAE, K., TSUDA, K., NAGASAWA, I. Non-ohmic properties of ZnO-rare earth metal oxide-$Co_3O_4$ ceramics. **Jpn. J. Appl. Phys.**, v.16, n.8, p. 1361-1368, 1977.
12 NAHM, C-W., PARK, C-H. Microstructure, electrical properties, and degradation behavior of praseodymium oxides-based zinc oxide varistors doped with $Y_2O_3$. **J. Mater. Sci.**, v.35, p. 3037-3042, 2000.
13 NAHM, C-W. Electrical properties and aging characteristics of terbium-doped ZPCC-based varistors **Mat. Sc. and Eng. B**, v.137, p. 112-118, 2007.
14 ZU, P., TANG, Z. K., WONG, G. K. L., KAWASAKI, M., OHTOMO, A., KOINUMA, H., SEGAWA, Y. Ultraviolet spontaneous and stimulated emissions from ZnO microcrystallite thin films at room temperature. **Solid State Commun.** 103, p. 459, 1997.
15 OHNISHI, T., OHTOMO, A., KAWASAKI, M., KOINUMA, H. Determination of surface polarity of c-axis oriented ZnO films by coaxial impact-collision ion scattering spectroscopy. **Appl. Phys. Lett.** 72, p. 824, 1998.
16 FURTADO, J. G. M., SALÉH, L. A., SERRA, E. T. Características microestruturais e estabilidade eletrotérmica de cerâmicas varistoras à base de óxido de zinco. **Proceedings of XVI CBECIMAT**, Porto Alegre, Brasil, 2004.
17 ARNOULD, X., COSTER, M., CHERMANT, J-L. Segmentation and Grain Size of Ceramics. **Image Anal Stereol.** 20, p. 131, 2001.
18 CHINN, R. Grain Sizes of Ceramics by Automatic Image Analysis. **J. Am. Ceram. Soc.**, v.77, n.2, p. 589-592, 1994.
19 FURTADO, J. G. M., SALÉH, L. A., SERRA, E. T., OLIVEIRA, G. S. G. Microstructural Evaluation of Rare-Earth-Zinc Oxide-Based Varistor Ceramics. M**aterials Research**, v.8, n. 4, p. 425-429, 2005.